Supplementary Figures and Tables

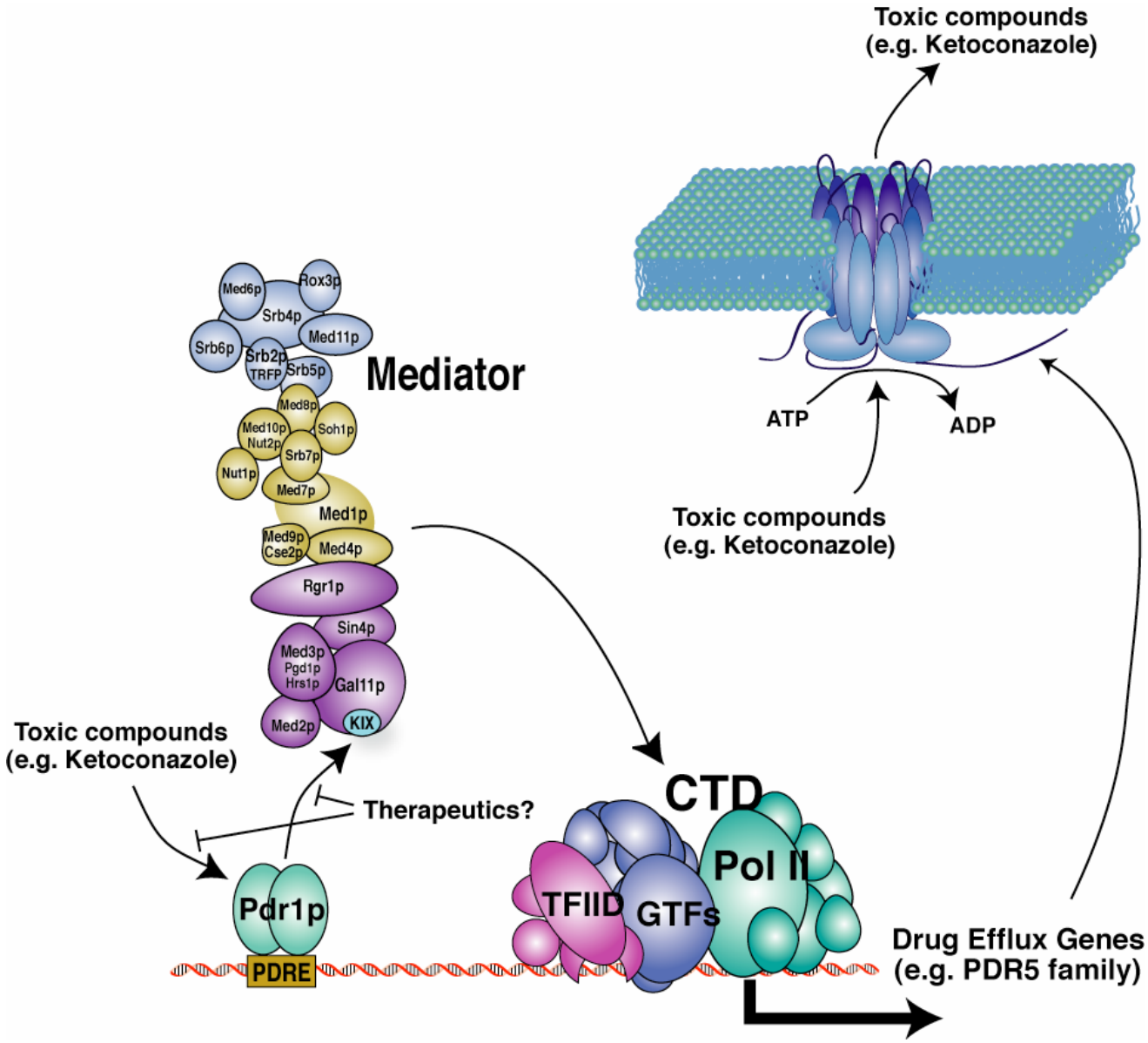

Supplementary Figure 1. Cartoon depicting hypothetical model of xenobiotic-dependent gene regulation of drug efflux pumps by Pdr1p orthologs in fungi. Pdr1p orthologs control the expression of genes encoding drug efflux pumps (e.g. ABC transporters) in response to direct binding of xenobiotics (e.g. ketoconazole) to a discrete ligand binding domain, allowing the activation domain to interact with the KIX domain of the Gal11p subunit of the Mediator co-activator. The Mediator in turn interacts with the C-terminal domain (CTD) of the large subunit of RNA polymerase II (Pol II) and facilitates recruitment of Pol II to Pdr1p target genes, allowing transcription. Based on the nuclear receptor paradigm (e.g. the identification of tamoxifen as an antagonist of estrogen receptor signaling in breast cancer treatment), we speculate that small-molecule inhibitors might be identified that interfere with either productive xenobiotic binding or with Gal11p KIX recruitment by Pdr1p orthologs in pathogenic fungi. Such agents could serve as precursors for therapeutics targeting the molecular basis for xenobiotic-stimulated MDR in the prevalent human pathogen *C. glabrata*.

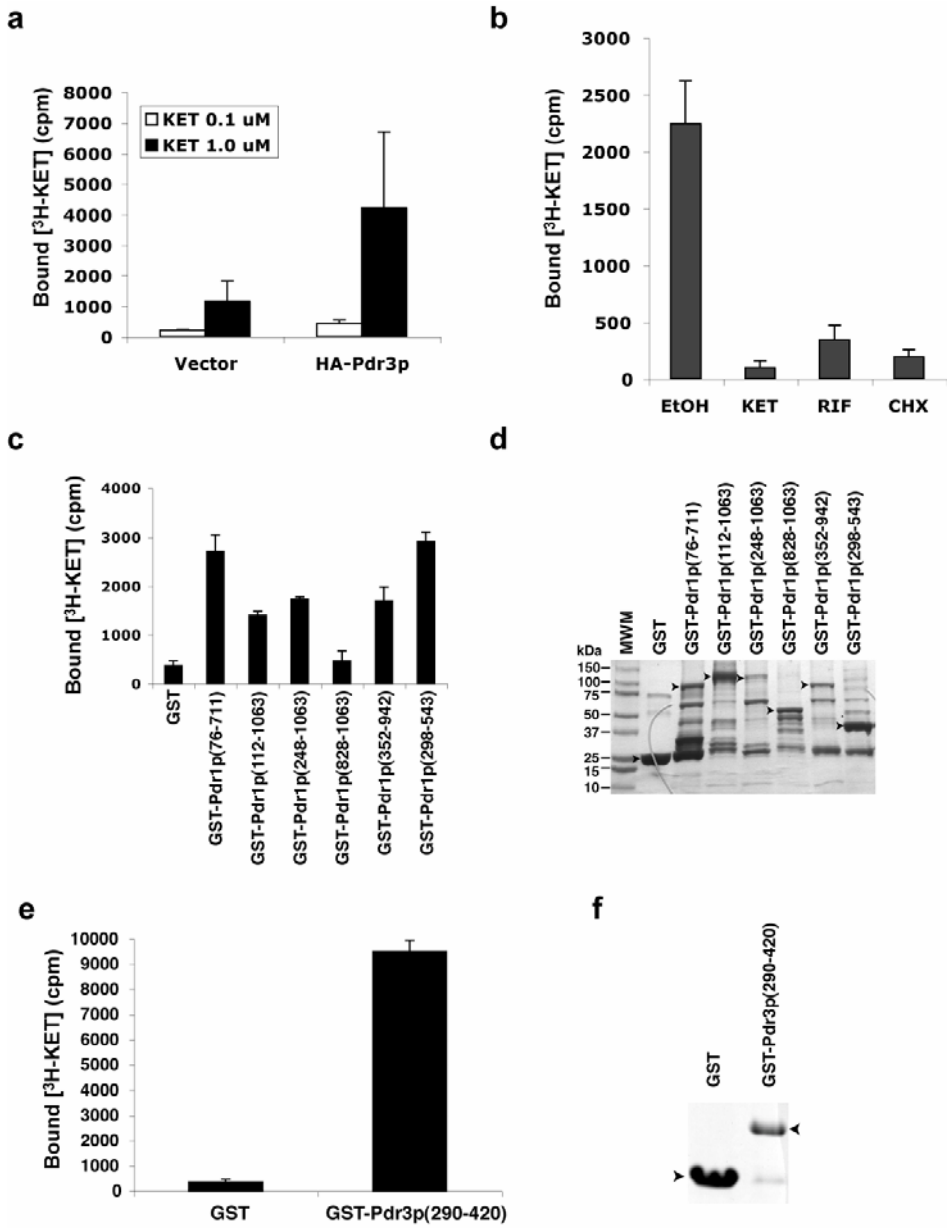

Supplementary Figure 2. Identification of Pdr1p and Pdr3p Xenobiotic Binding Domains. a, Binding of radiolabeled ketoconazole to Pdr3p. Protein A-sepharose/antibody beads with immunopurified HA (vector) or HA-Pdr3p proteins were used for direct binding with radiolabeled ketoconazole. Binding experiments were performed in triplicates. Mean values are shown and error bars represent standard deviation. **b,** Cold competition assay indicates that other xenobiotics (rifampicin and cycloheximide) also bind to Pdr3p. Unlabelled xenobiotics (X-axis) were used at 1000-fold excess of radiolabeled ketoconazole (0.1 μM). **c,** Binding of ^{3}H-KET with various GST-Pdr1p fragments shows that the minimal region required for xenobiotic binding resides in a fragment of aa 352-543. Glutathione sepharose beads with GST alone or different GST-Pdr1p proteins were used for direct binding with radiolabeled ketoconazole. Mean values from three independent replicates are shown, and error bars represent standard deviation. **d,** Expression of GST-Pdr1p proteins used in A. as visualized by Coomassie stained gel. Arrows indicate full-length GST-fusion proteins. **e,** Identification of xenobiotic binding domain in Pdr3p. Glutathione sepharose beads with purified GST-Pdr3p (aa 290-420) recombinant protein were used for direct binding with radiolabeled ketoconazole. Beads with GST alone were used as control. Binding assays were performed in triplicate. Mean values are shown and error bars represent standard deviation. **f,** Expression of GST and GST-Pdr3p (aa 290-420) proteins used in **e,** as visualized by Coomassie staining.

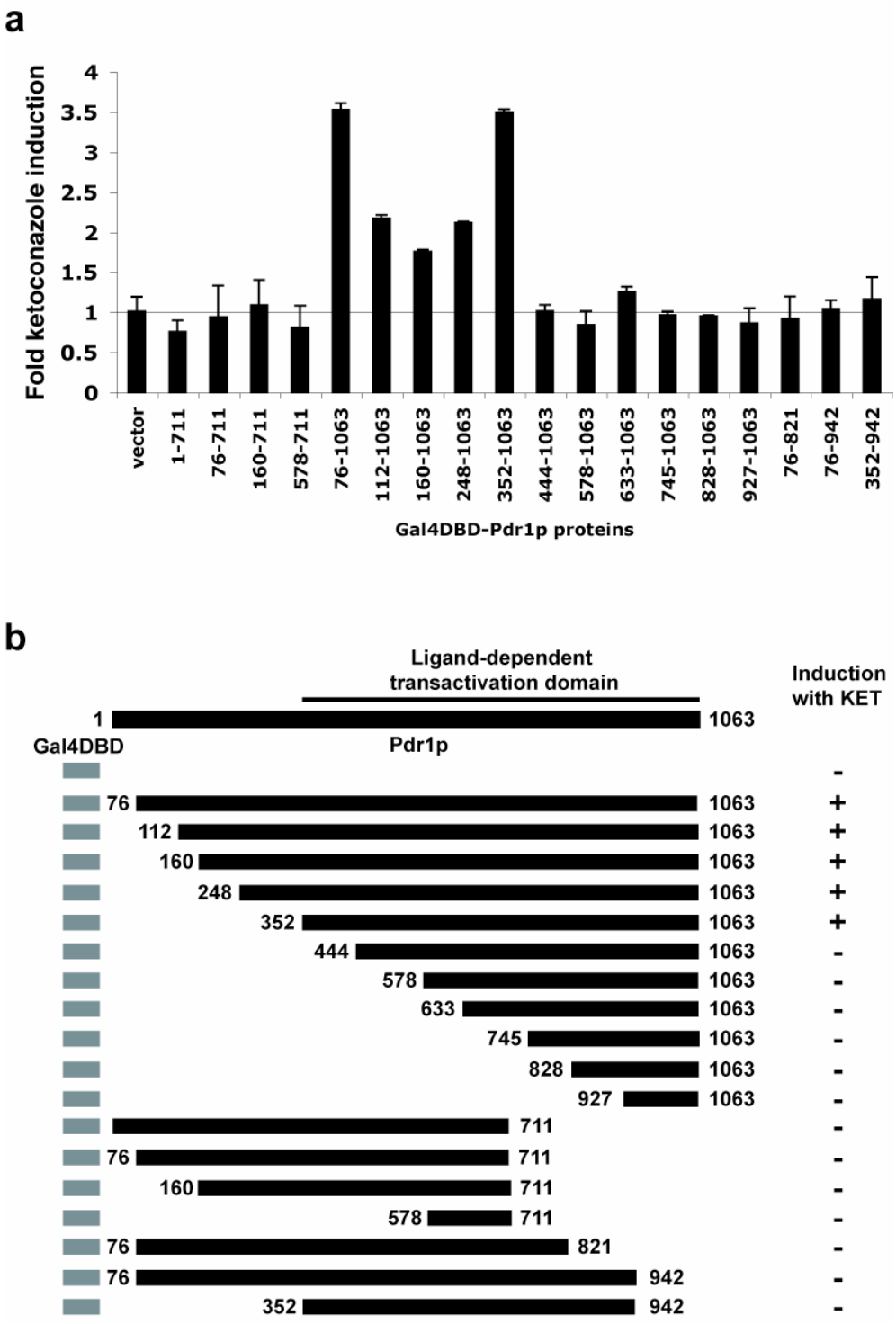

Supplementary Figure 3. Characterization of a Transferable Xenobiotic-Responsive Domain in Pdr1p. **a,** β-galactosidase assay shows that a large carboxyl-terminal region (aa 352-1063) possesses a transferable xenobiotic-responsive transactivation domain. Yeast cells with an integrated *GAL7*-LacZ reporter were transformed with plasmids harboring the Gal4DBD-PDR1 recombinant cDNAs (X-axis), treated with ketoconazole or ethanol (vehicle), and used for β-galactosidase assays. β-galactosidase activity from ketoconazole-treated samples were divided by that from ethanol samples and presented as fold induction on Y-axis. Mean values from three replicate experiments are shown, and error bars represent standard deviation. **b,** Summary of the data in **a**. '+' signs indicate induction (> 1.5-fold) of *GAL7*-LacZ reporter expression in response to ketoconazole, whereas '-' sign indicate no response.

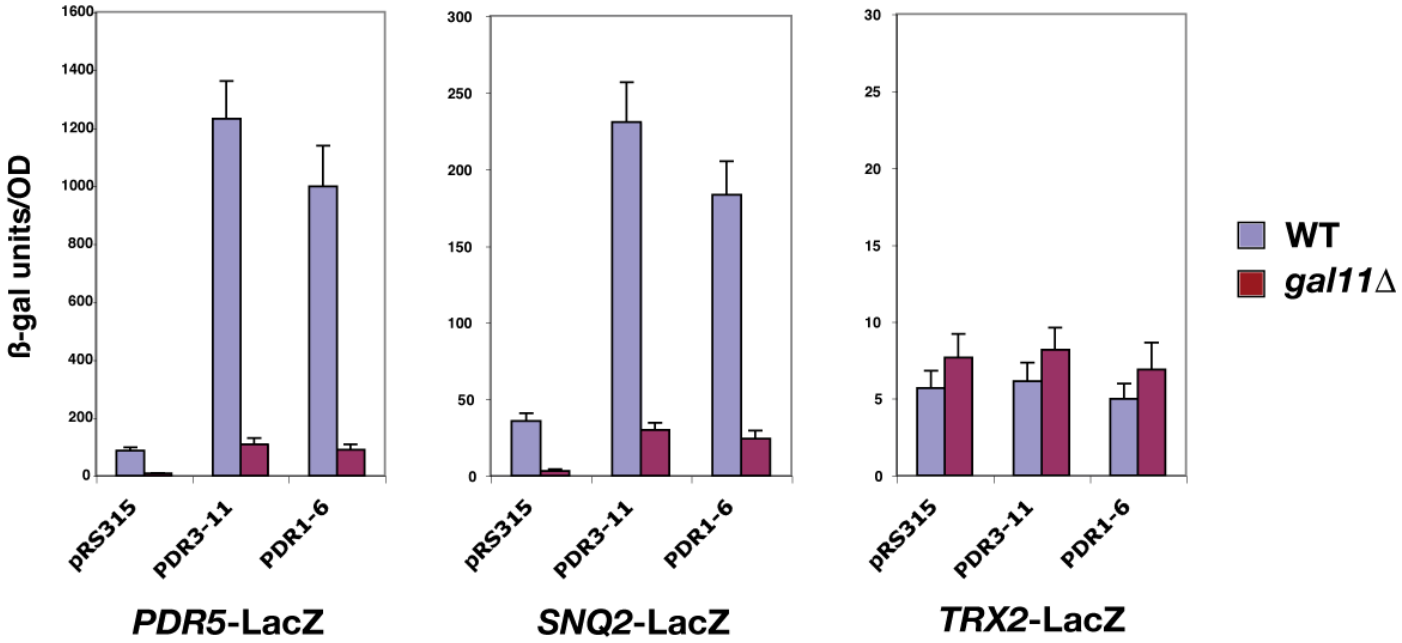

Supplementary Figure 4. Requirement of Gal11p for the Expression of Pdr1p/Pdr3p Target Promoters. WT and *gal11*Δ yeast strains that express constitutively active forms of Pdr1p (PDR1-6), Pdr3p (PDR3-11), or control vector (pRS315) were transformed with plasmids harboring the LacZ gene under the control of the *PDR5*, *SNQ2*, or *TRX2* (control) promoters and transcriptional activity was assessed by β-galactosidase assays. Mean value from three replicates are shown. Error bars represent standard deviation.

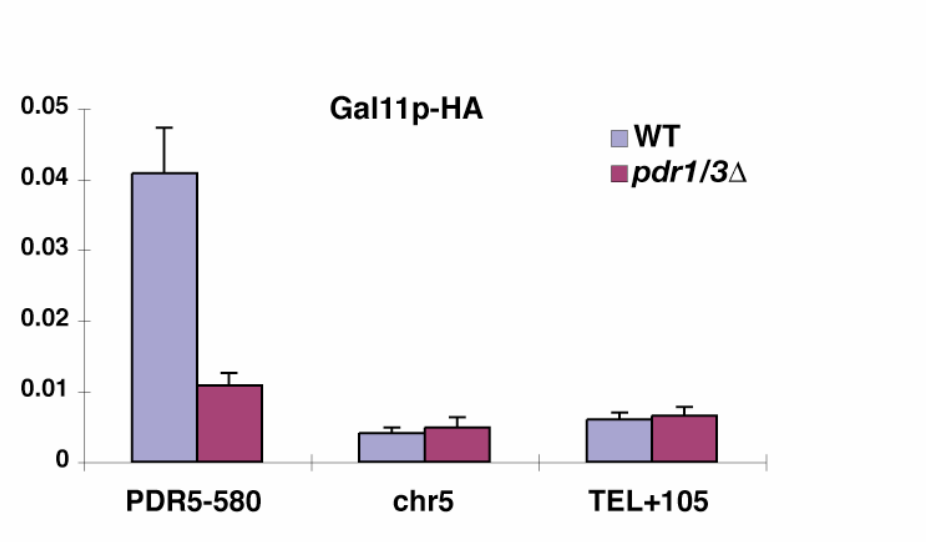

Supplementary Figure 5. Gal11p recruitment to the Pdr1p/Pdr3p target gene *PDR5 in vivo*. Chromatin immunoprecipitation analysis shows that HA-Gal11p occupancy on the *PDR5* promoter (PDR5-580) is Pdr1p/Pdr3p-dependent. No significant association of HA-Gal11p with control genomic regions (chr5 and TEL+105) was observed.

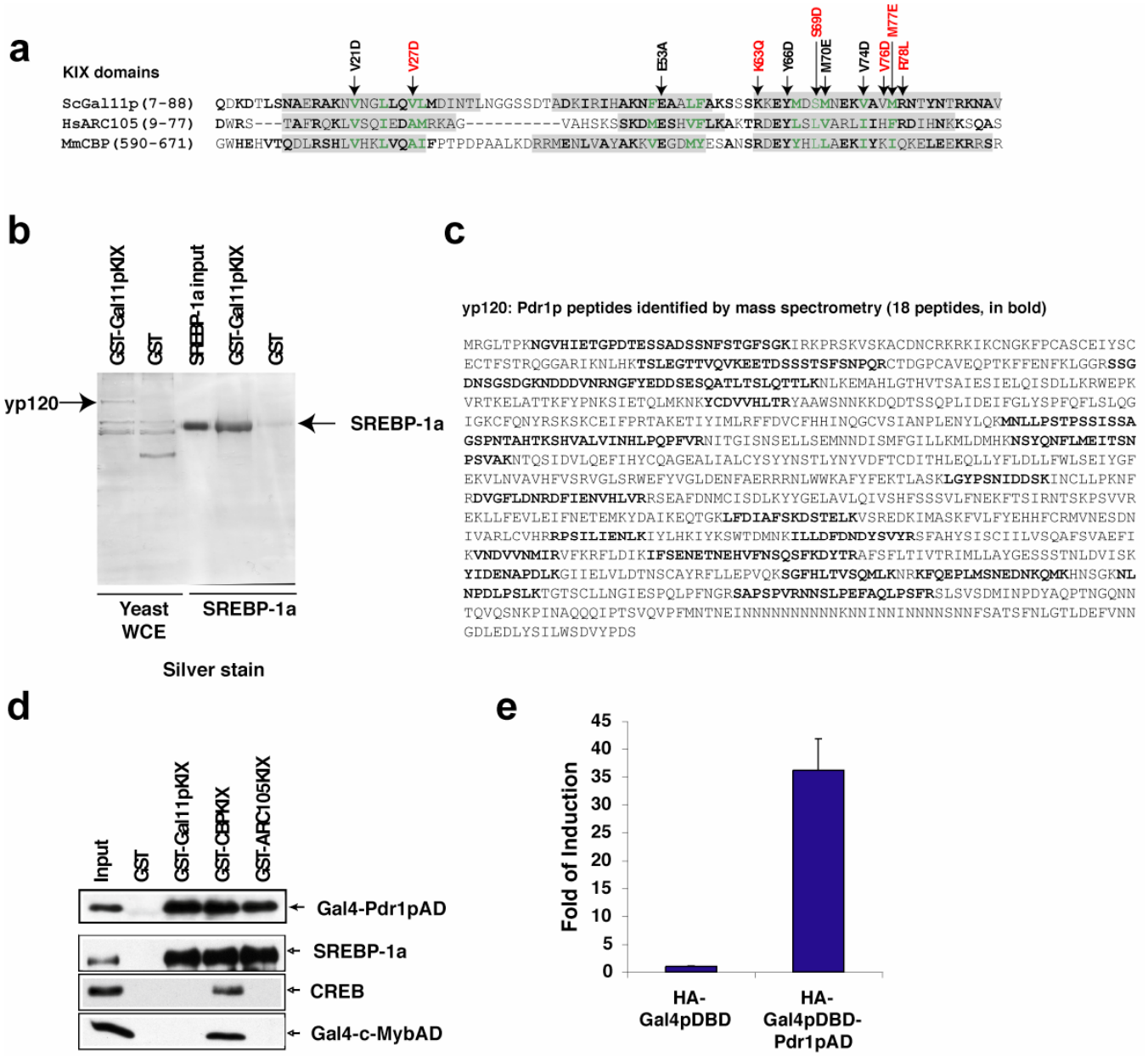

Supplementary Figure 6. Interaction Between the Gal11p KIX Domain and the Pdr1p AD. a, Sequence alignment shows the similarity (in bold) between the yeast (Sc) Gal11p KIX domain and the KIX domains of human (Hs) ARC105/MED15 and mouse (Mm) CBP co-activators. Conserved hydrophobic amino acids are highlighted in green. Helices are indicated by gray boxes. The point-mutated amino acids in the Gal11p KIX domain are indicated by arrows, with mutations that affect binding with Pdr1p in red. **b,** GST-pulldown reveals that Gal11p KIX specifically interacts with a yeast protein with an approximate molecular weight of 120 kDa. Like human ARC105 and CBP KIX domains, yeast Gal11p KIX can interact with SREBP-1a (Yang et al. 2006). Glutathione sepharose beads with GST alone were used as control. **c,** Peptide microsequencing by mass spectrometry indicates that the 120 kDa yeast protein interacting with Gal11p KIX is Pdr1p. The peptides, which were identified by mass spectrometry, are shown in bold. **d,** GST-pulldown assay shows interaction between GST-KIX domain fusion proteins and the Pdr1p activation domain (AD, amino acids 966-1068) fused to the Gal4p DBD. Recombinant human SREBP-1a also interacts with all three KIX domains. In contrast, PKA-phosphorylated CREB or Gal4-c-MybAD only bound to the CBP KIX domain. **e,** The Pdr1pAD (amino acids 966-1068) fused to Gal4pDBD is functional in mammalian cells (HEK293T), as revealed by Luciferase reporter assays. Gal4pDBD alone was used as control. Mean value from triplicate experiments are shown, and the error bars represent standard deviation.

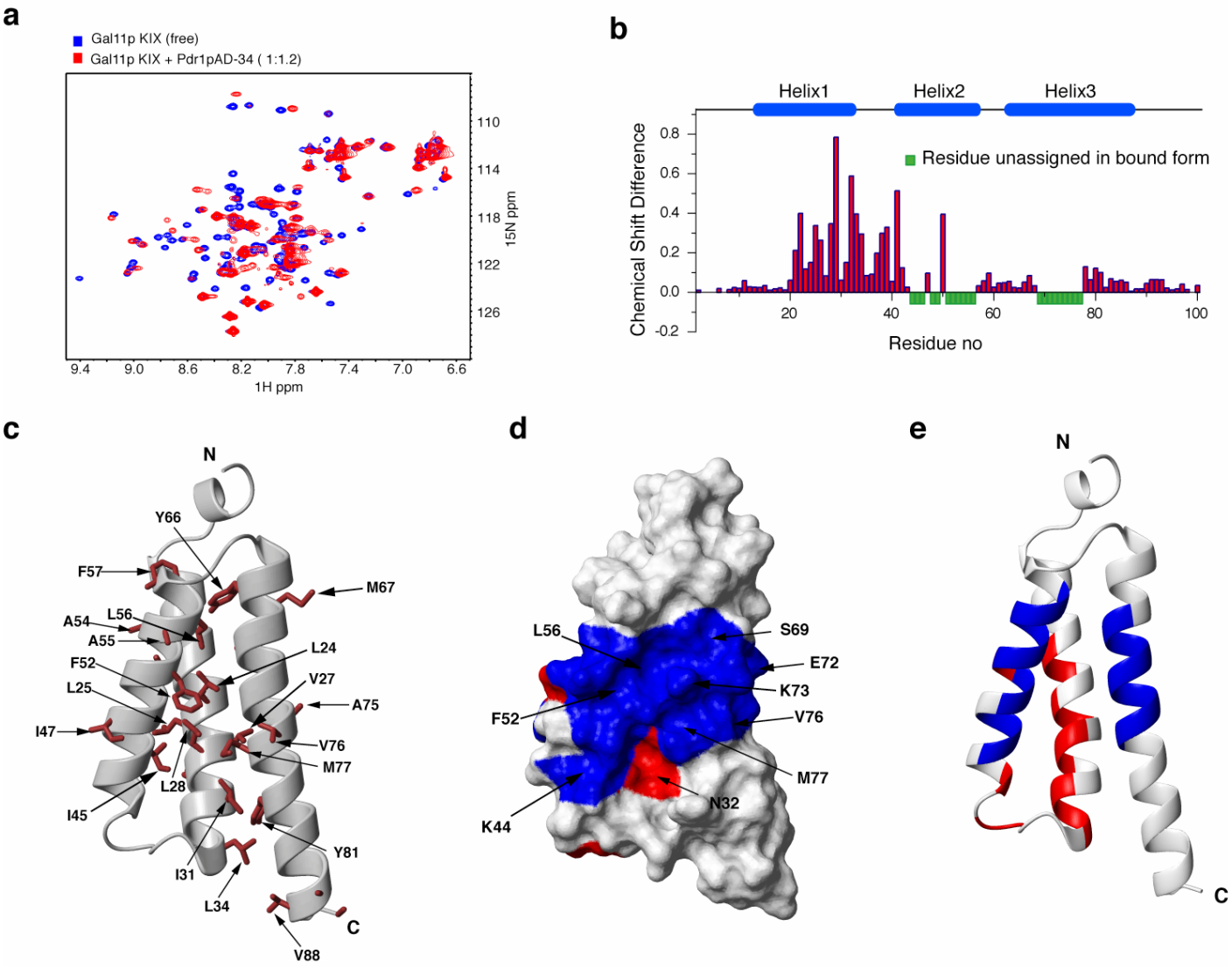

Supplementary Figure 7. Analysis of the interaction of Gal11p KIX with a 34-amino acid Pdr1p activation domain fragment. a, An overlay of HSQC spectrum of Gal11p KIX in blue and a complex of Gal11p KIX and unlabelled Pdr1pAD-34 (in the molar ratio of 1:1.2) in red. The spectrum reveals substantial changes in the chemical shift of Gal11p KIX upon binding Pdr1pAD-34. **b,** The plot shows the chemical shift changes (represented by $((\Delta N/5)^2 + (\Delta HN)^2)^{0.5}$) of Gal11p KIX upon binding Pdr1pAD-34 as a function of residue number. Green bars indicate that the residue was not assigned in the bound form. **c,** Ribbon representation of Gal11p KIX with the side chain residues of the hydrophobic core highlighted in stick diagram. **d,** Surface representation of Gal11p KIX with the surface interacting with Pdr1pAD-34 (molar ratio 1:1.2 Gal11p KIX:Pdr1pAD-34) shown in red and blue. The residues shown in red correspond to a chemical shift change of more than 0.2 ppm. The residues shown in blue move substantially and/or broaden upon binding to Pdr1pAD-34, which prohibits their assignment in the bound form. **e,** Ribbon representation of the analysis in **d**.

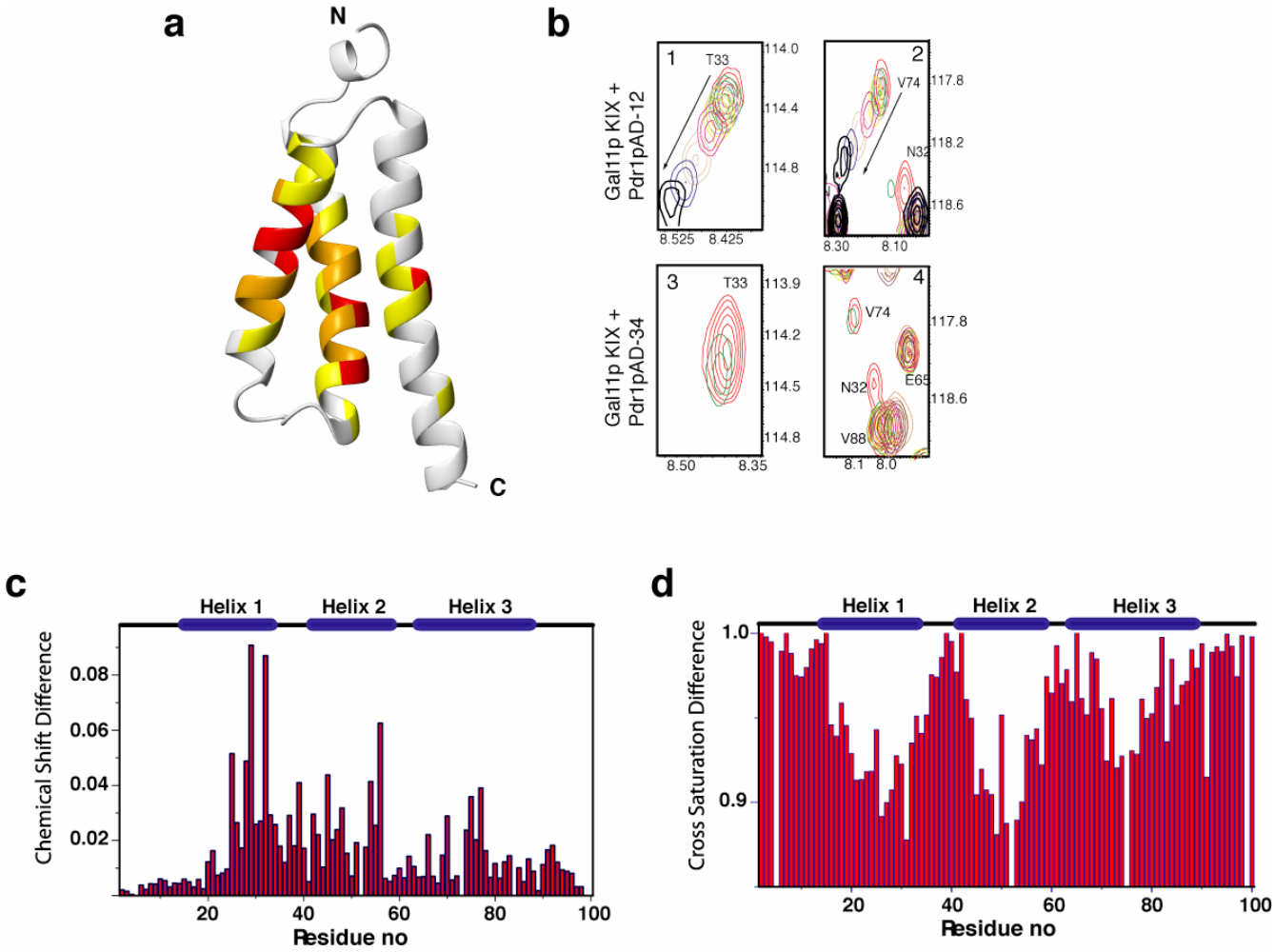

Supplementary Figure 8. NMR analysis of the interaction of Gal11p KIX with Pdr1pAD fragments. a, Ribbon representation showing the residues affected by cross saturation difference experiments. Yellow, orange, and red represent weak, medium, and strong effects, respectively, as observed by cross saturation experiments carried out on a perdeuterated sample of Gal11p KIX in complex with Pdr1pAD-12 in the molar ratio 5:1. **b,** Titration of Gal11p KIX with Pdr1pAD-12 followed by HSQC analysis. The colors red, green, yellow, pink, coral, blue, and black represent molar ratios of 10:0, 10:1, 4:1, 2:1, 1:1, 1:4, 1:10 of Gal11p KIX:Pdr1pAD-12 peptide, respectively. Panels 1 and 2 show the chemical shift change of residue T33 and V74 when Gal11p KIX is titrated with Pdr1pAD-12, whereas panels 3 and 4 show the chemical shift change for the same residues when titrated with Pdr1pAD-34. In the case of Pdr1pAD-12, the resonances are in fast exchange moving steadily from the free to bound state during the course of the titration, but some line broadening is also observed. In the case of Pdr1pAD-34, the resonances disappear during the course of titration, which is representative of intermediate exchange. **c,** Chemical shift difference (represented by $((\Delta N/5)^2 + (\Delta HN)^2)^{0.5}$) between free Gal11p KIX and a complex of Gal11p KIX with Pdr1pAD-12 in the molar ratio 5:1. **d,** Cross saturation difference (ratio of saturated to non-saturated) of a complex of Gal11p KIX with Pdr1pAD-12 in the molar ratio 5:1.

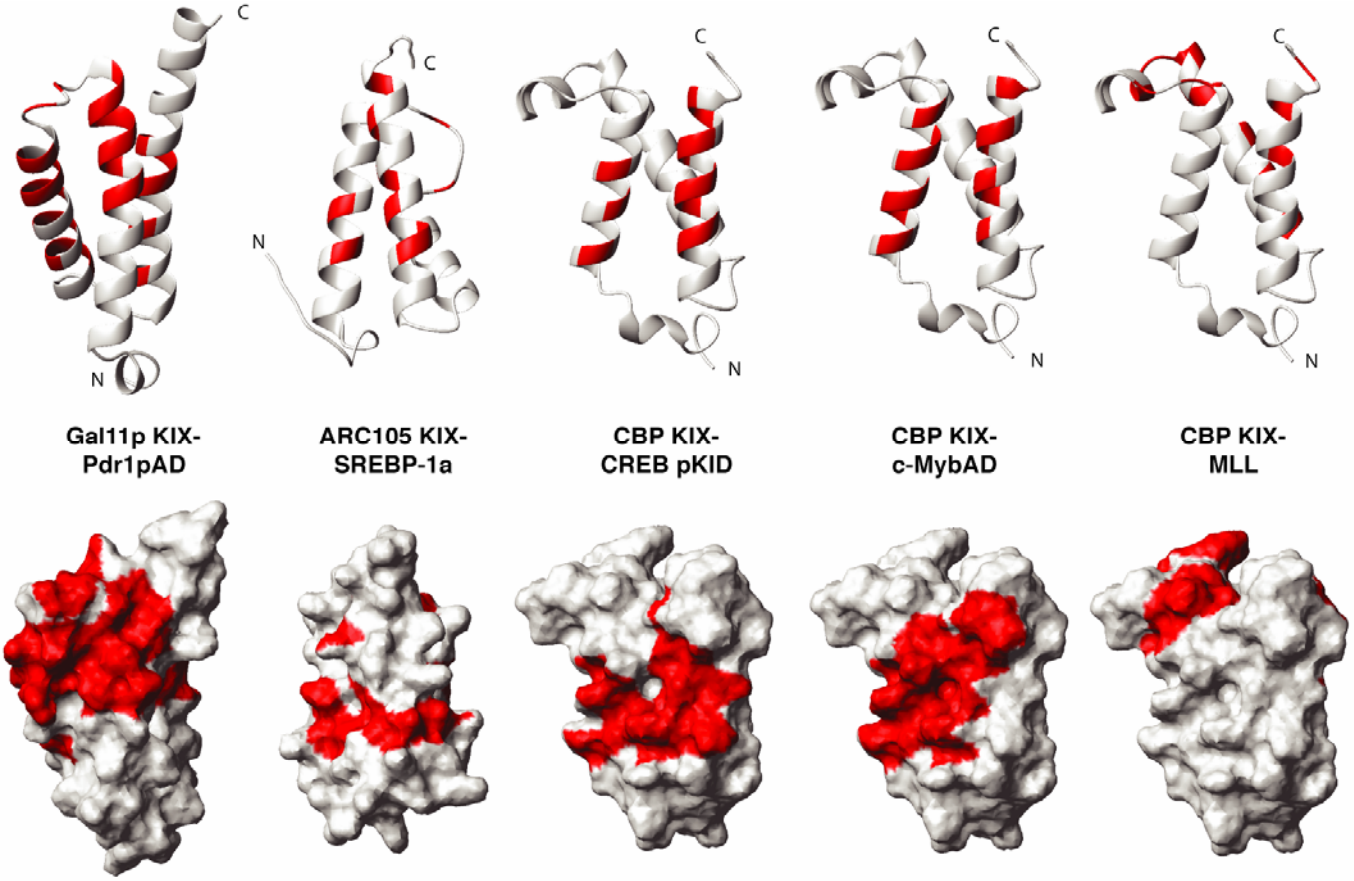

Supplementary Figure 9. Comparison of activator binding sites on KIX domains. Top: From the left, ribbon representations of yeast Gal11p KIX bound to the Pdr1pAD-12, human ARC105/MED15 KIX bound to the SREBP-1a AD-26, and mouse CBP KIX bound to CREB pKID, c-MybAD, and MLL, respectively. The activation domain binding sites are highlighted in red. **Bottom:** Surface representations of the KIX domains with the activator binding sites in red.

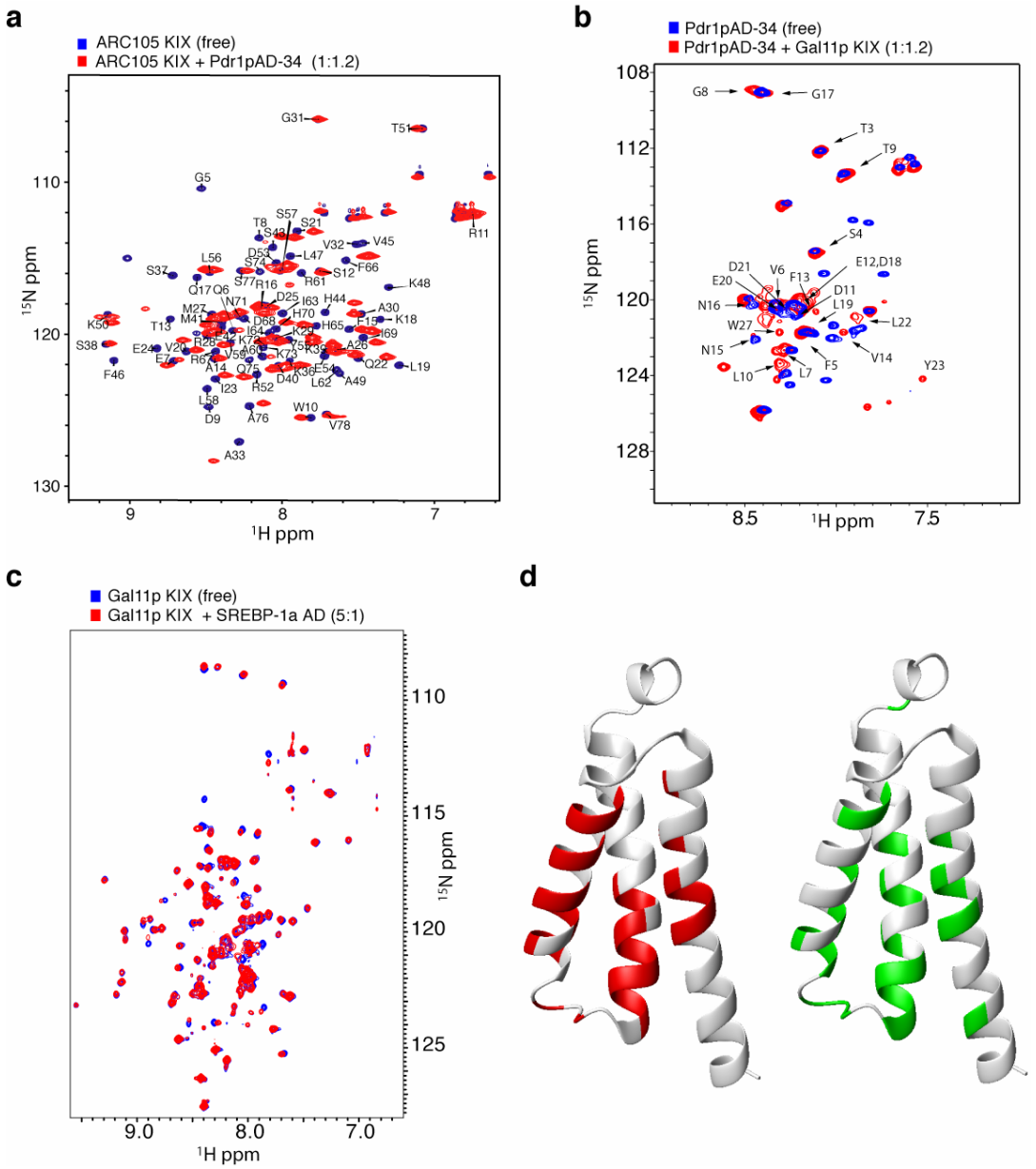

Supplementary Figure 10. NMR analysis of Pdr1pAD and SREBP-1aAD interaction with Gal11p and ARC105/MED15 KIX domains. a, An overlay of the HSQC spectrum of free ARC105 KIX (blue) and ARC105 KIX with Pdr1pAD-34 in the molar ratio 1:1.2 (red). **b,** An overlay of the HSQC spectrum of Pdr1pAD-34 in blue and a complex of Pdr1pAD-34 and unlabelled Gal11p KIX (in the molar ratio of 1:1.2) in red. **c,** An overlay of the HSQC spectrum of Gal11p-KIX in blue and a complex of Gal11p-KIX and unlabelled SREBP1aAD(1-26) (in the molar ratio of 5:1) in red. **d,** Ribbon representation of Gal11p KIX where residues shown in red (left) and green (right) correspond to a chemical shift change (represented by $((\Delta N/5)^2 + (\Delta HN)^2)^{0.5}$) of more than 0.02 ppm upon addition of Pdr1pAD-12 and SREBP-1aAD(1-26) respectively (molar ratio of 5:1 Gal11p KIX:peptide).

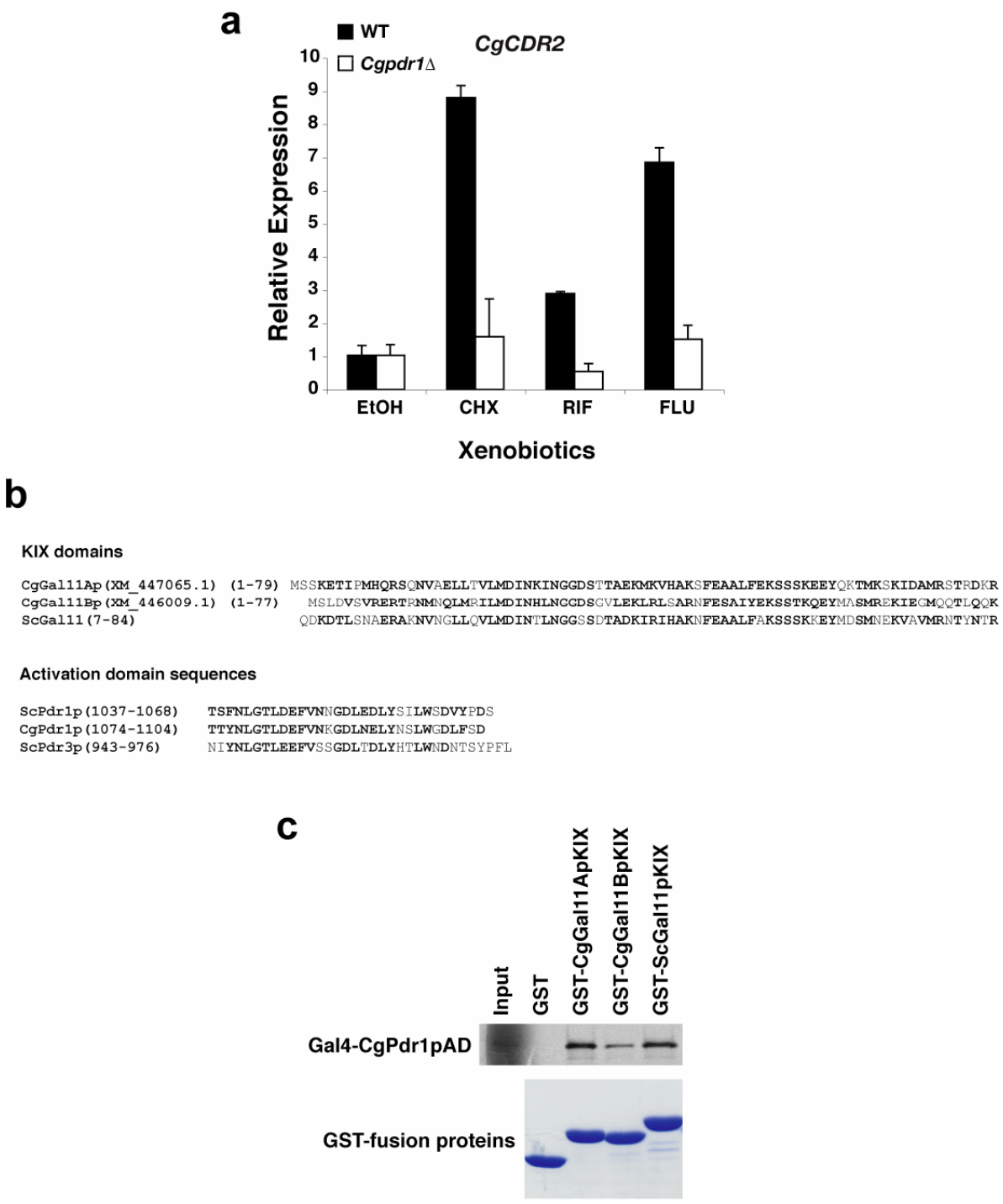

Supplementary Figure 11. **Requirement of CgPdr1p in xenobiotic-stimulated transactivation and binding studies of Gal4-CgPdr1pAD with KIX domains from CgGal11Ap.** CgGal11Bp, and ScGal11p. **a,** Xenobiotic-induced expression of *CgCDR2* is largely CgPdr1p-dependent. Quantitative RT-PCR analysis was performed in triplicate. Mean values are shown, and the error bars represent standard deviation. **b,** Top: Sequence alignment of *S. cerevisiae* (Sc) and *C. glabrata* (Cg) KIX domains. Similarities are highlighted in bold. Bottom: Sequence alignment shows the similarity (in bold) between the C-terminal activation domains of *S. cerevisiae* (Sc) and *C. glabrata* (Cg) Pdr1p/Pdr3p orthologs. **c,** GST-pulldown analysis shows that the interaction of ^{35}S-Met labeled Gal4DBD-CgPdr1pAD with KIX domains of CgGal11Ap and ScGal11p is significantly stronger than with the CgGal11Bp KIX domain. GST alone were used as control. Upper panel shows the interacting proteins, whereas bottom panel shows the GST-fusion proteins as assessed by Coomassie staining.

Supplementary Table 1. Strains used in this study

Strain	Genotype	Reference
WT BY4741	MATa *his3*Δ1 *leu2*Δ0 *met15*Δ0 *ura3*Δ0	Giaever et al. 2002
WT SEY6210	Matα leu2-3,-112 ura3-52 lys2-801 trp1-Δ901 his3-Δ 200 suc2-Δ9 Mel1	Scott Emr
*pdr1*Δ	SEY6210 *pdr1*Δ	Scott Moye-Rowley
*pdr3*Δ	SEY6210 *pdr3*Δ	Scott Moye-Rowley
pdr1/3Δ	SEY6210 *pdr1*Δ *pdr3*Δ	Scott Moye-Rowley
*yap1*Δ	SEY6210 yap1Δ	Scott Moye-Rowley
*rox3*Δ	SEY6210 *rox3*Δ	Scott Moye-Rowley
*gal11*Δ	SEY6210 *gal11*Δ	Scott Moye-Rowley
*med2*Δ	SEY6210 *med2*Δ	Scott Moye-Rowley
*rox3*Δ	BY4741 *rox3*Δ	Kevin Struhl
*med2*Δ	BY4741 *med2*Δ	Kevin Struhl
*nut1*Δ	BY4741 *nut1*Δ	Kevin Struhl
*ssn2*Δ	BY4741 *ssn2*Δ	Kevin Struhl
*srb8*Δ	BY4741 *srb8*Δ	Kevin Struhl
*cse2*Δ	BY4741 *cse2*Δ	Kevin Struhl
*ssn8*Δ	BY4741 *ssn8*Δ	Kevin Struhl
*pgd1*Δ	BY4741 *pgd1*Δ	Kevin Struhl
*med1*Δ	BY4741 *med1*Δ	Kevin Struhl
*soh1*Δ	BY4741 *soh1*Δ	Kevin Struhl
*sin4*Δ	BY4741 *sin4*Δ	Kevin Struhl
*srb5*Δ	BY4741 *srb5*Δ	Kevin Struhl
*gal11*Δ	BY4741 *gal11*Δ	Kevin Struhl
CgBG2WT	Wild-type	Cormack & Falkow, 1999
CgBG14	*ura3*Δ::*Tn903* G418^R	Cormack & Falkow, 1999
*Cgpdr1*Δ (BG1712)	*ura3*Δ::*Tn903* G418^R *pdr1*Δ	This study
*Cggal11A*Δ (BG1710)	*ura3*Δ::*Tn903* G418^R *gal11a*Δ	This study
*Cggal11B*Δ (BG1711)	*ura3*Δ::*Tn903* G418^R *gal11b*Δ	This study
*Cgmed1*Δ (BG1713)	*ura3*Δ::*Tn903* G418^R *med1*Δ	This study
*Cggal11A/B*Δ (BG1725)	*ura3*Δ::*Tn903* G418^R *gal11a*Δ *gal11b*Δ::*hph* Hyg^R	This study
*Cgpdr1*Δ (BG1719)	*URA3 pdr1*Δ	This study
*Cggal11A*Δ (BG1718)	*URA3 gal11a*Δ	This study
*Cggal11B*Δ (BG1721)	*URA3 gal11b*Δ	This study
*Cgmed1*Δ (BG1720)	*URA3 med1*Δ	This study
*Cggal11A/B*Δ (BG1726)	*URA3 gal11a*Δ *gal11b*Δ::*hph* Hyg^R	This study

Supplementary Table 2. List of primers used for quantitative real-time RT-PCR

ScPDR5	Forward	5' ACTTCTGGATTGTTTGGCCG 3'
	Reverse	5' CTCAATGACTCCCTCACAGTGG 3'
ScPDR16	Forward	5' AATAACTGCTGACTTGGTGGCC 3'
	Reverse	5' CCAACATGAAGACCAAGTGCTG 3'
ScACT	Forward	5' CTCCGTCTGGATTGGTGGTTCT 3'
	Reverse	5' CGCGCACAAAAGCAGAGATTA 3'
CgCDR2	Forward	5' AAGGTGCCAAACAGAAAGGTGA 3'
	Reverse	5' TGGTCGCATTGGAGGTTATAGA 3'
CgACT	Forward	5' CTCCACCACTGCTGAAAGAG 3'
	Reverse	5'GGTCAATACCAGCAGATTCTAG 3'

Supplementary Table 3. Statistics for the final 20 NMR structures of Gal11p KIX

Number of NOE distance constraints	
Total	1359
Intra-residue	254
Short and Medium (|i-j| = 1 ~ 4)	1039
Long (|i-j| > 4)	66
Backbone angular restraints (ϕ and φ)	146
Violations (mean and s.d.)	
Distance constraints (Å)	0.0179±0.0009
Dihedral angle constraints (º)	0.6305±0.0767
Max. dihedral angle violation (º)	4.93
Max. distance constraint violation (Å)	0.36
Ramachandran Plot (20 structures)	
Residues in most favored region (%)	92.4
Residues in additionally allowed region (%)	4.9
Residues in generously allowed and disallowed region (%)	1.7
Residues in disallowed region (%)	1.1
G-factors	
Mainchain dihedral angles	0.14
χ^1 dihedral angles	-1.24
χ^1/ χ^2 dihedral angles	-0.45
Average RMSD to mean (20 structures)	
Backbone (N, Ca, C)	0.60 ± 0.15
All heavy atoms	1.00 ± 0.15

[a]None of these 20 structures exhibited distance violations >0.5 Å or dihedral angle violations >5°. There are no bad contacts in the structures. The RMSD for covalent bonds and angles relative to the standard dictionary is 0.005 Å and 0.6 degrees, respectively, with all covalent bonds and angles within 6.0*RMSD for the structures.
[b]The program PROCHECK-NMR (Laskowski et al., 1996) was used to assess the stereochemical quality of the structures.

Reference:
Laskowski, R.A., *et al.* AQUA and PROCHECK-NMR: Programs for checking the quality of protein structures solved by NMR. *J. Biomol. NMR* **8**, 477-486 (1996).